Inorganic Chemistry

Article

pubs.acs.org/IC

Impact of Ligand Modification on Hydrogen Photogeneration and Light-Harvesting Applications Using Cyclometalated Iridium Complexes

Yong-Jun Yuan,[†] Ji-Yuan Zhang,[†] Zhen-Tao Yu,*[,†,‡] Jian-Yong Feng,[†] Wen-Jun Luo,[†] Jin-Hua Ye,[§] and Zhi-Gang Zou*[,†]

[†]Eco-Materials and Renewable Energy Research Center, National Laboratory of Solid State Mircrostructures, Department of Materials Science and Engineering, Nanjing University, Nanjing 210093, P. R. China

[‡]State Key Laboratory of Coordination Chemistry, Nanjing University, Nanjing 210093, P. R. China

[§]Photocatalytic Materials Center, National Institute for Materials Science, Sengen, Tsukuba, Ibaraki 305-0047, Japan

Supporting Information

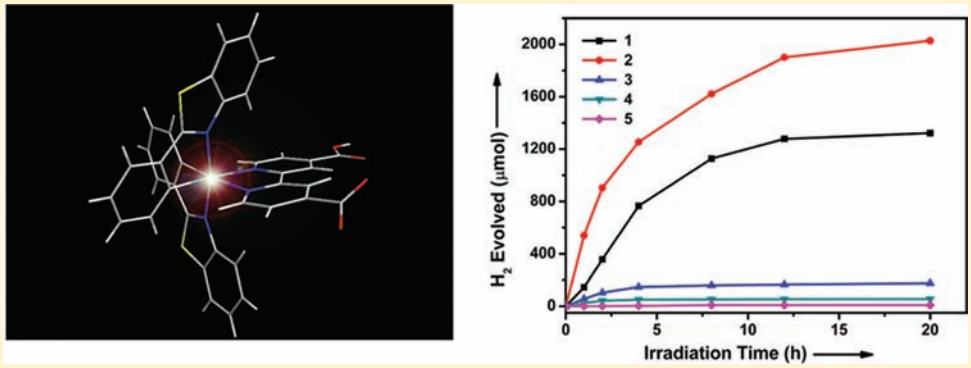

ABSTRACT: To explore structure−activity relationships with respect to light-harvesting behavior, a family of bis-cyclometalated iridium complexes $[Ir(C^N)_2(Hbpdc)]$ **2**−**5** (where C^N = 2-phenylbenzothiazole and its functionalized derivatives, and H_2bpdc =2,2′-bipyridine-4,4′-dicarboxylate) was synthesized using a facile method. The photophysical and electrochemical properties of these complexes were investigated and compared to those of analogue **1** (C^N = (4-trifluoromethyl)-2-phenylbenzothiazole); they were also investigated theoretically using density functional theory. The molecular structures of complexes **2**−**4** were determined by X-ray crystallography, which revealed typical octahedral coordination geometry. The structural modifications involved in the complexes were accomplished through the attributes of electron-withdrawing CF_3 and electron-donating NMe_2 substituents. The UV−vis spectra of these species, except for that of **5**, displayed a broad absorption in the low-energy region, which originated from metal-to-ligand charge-transfer transitions. These complexes were found to exhibit visible-light-induced hydrogen production and light-to-electricity conversion in photoelectrochemical cells. The yield of hydrogen production from water using these complexes was compared, which revealed substantial dependences on their structures, particularly on the substituent of the cyclometalated ligand. Among the systems, the highest turnover number of 1501 was achieved with complex **2**, in which the electron-withdrawing CF_3 substituent was connected to a phenyl ring of the cyclometalated ligand. The carboxylate anchoring groups made the complexes highly suitable for grafting onto TiO_2 (P25) surfaces for efficient electron transfer and thus resulted in an enhancement of hydrogen evolution compared to the unattached homogeneous systems. In addition, the combined incorporation of the electron-donating NMe_2 group and the electron-withdrawing CF_3 substituent on the cyclometalated ligand caused complex **5** to not work well for hydrogen production. Their incorporation, however, enhanced the performance of **5** in the light-harvesting application in nanocrystalline TiO_2 dye-sensitized solar cells, which was attributed to the intense absorption in the visible region.

INTRODUCTION

The conversion of solar energy into stored chemical and electrical energy represents an especially attractive solution for both the ever-increasing demand for energy and climate change because of the processes in which energy can be generated and utilized in an ecofriendly way.[1] Molecular architectures that mimic natural photosynthetic light-harvesting machinery to accomplish hydrogen production from the photocatalytic splitting of water are expected to make decisive contributions to address these concerns.[2−4] In this regard, transition-metal complexes that undergo intense absorption and exhibit long-

Received: November 11, 2011
Published: March 21, 2012

   dx.doi.org/10.1021/ic202423y | *Inorg. Chem.* 2012, 51, 4123−4133

Scheme 1. Cyclometalating Ligands Used for Functional $[Ir(C^N)_2(Hbpdc)]$ Complexes 1−5 Studied Here

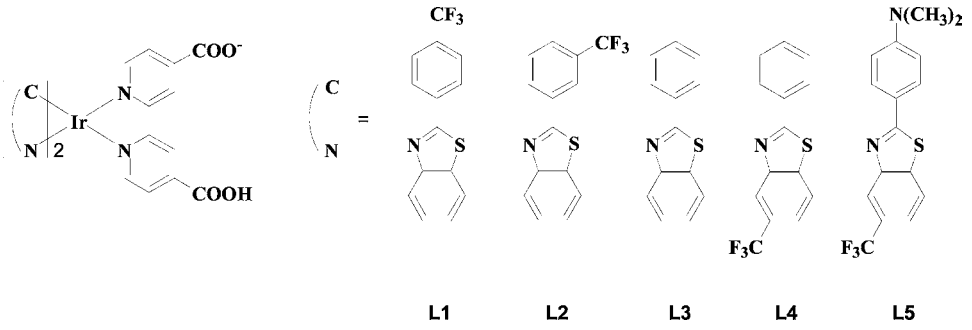

lived excited states have become increasingly desirable targets as photosensitizers (PSs) to harvest the energy of the sun and to carry out this reaction with a high efficiency.[5,6] Although a number of elaborate systems have been developed for the photogeneration of hydrogen in organic solutions with very small amounts of water, these systems suffer from low quantum efficiencies in aqueous media due to the poor solubility of PSs in water.[7] In contrast to this process, a semiconductor photocatalyst linked electronically to a light-capturing molecular moiety has been shown to efficiently generate electricity at low cost in a dye-sensitized solar cell (DSSC).[8] In this way, hybrid materials based on TiO_2 nanoparticles overcome some of the most important limitations intrinsic to wide-band-gap oxide semiconductors while maintaining the combined physical and chemical advantages of organic−inorganic hybrid assemblies. In these cells, most attention has been directed toward the use of metal ruthenium polypyridyl complexes that contain the labile Ru-NCS bond, which exhibit outstanding performance. However, with respect to the future prospects of DSSCs with metal complexes, the long-term ability of dyes is greatly hampered by the liberation of the NCS^- ligands from the metal center and by toxicity considerations.[9] Therefore, the development of PS dyes with controlled structures and the enhancement of their stability through chemical strategies is highly desired for the photoelectrochemical conversion of solar energy.

Apart from the ruthenium system, the exploration of charge-transfer complexes has only recently been extended to isoelectronic d^6-metal iridium complexes. Indeed, these luminescent complexes—in particular, cationic heteroleptic complexes of the kind of $[Ir(C^N)_2(N^N)]^+$ with C^N cyclometalating and N^N neutral ancillary diimine ligands—have been established as attractive materials for various optoelectronic applications because of their stability and because of the excellent and highly tunable electro-optical characteristics that arise from metal-to-ligand charge transfer (MLCT) transitions in these organometallics.[10,11] In addition, with respect to the long-lived triplet excited states, iridium light-harvesting complexes have demonstrated promising qualities in the efficient photoinduced charge separation for solar energy conversion because they exhibit high efficacy.[12] For this purpose, their ability to absorb visible light and to form highly energetic charge-separated excited states generated through MLCT transitions is crucial. Nevertheless, the development of the photochemistry of these complexes is limited by their weak absorption in the visible region. Therefore, changing the electronic density of the substituents on the attached ligands to produce iridium complexes that feature intense absorption and a broader spectral response in the visible region would seem to be warranted to achieve better light-harvesting performance and to therefore improve the performance of these materials. However, the weak metal−ligand bond in the cationic tris-diimine ruthenium complexes can be easily broken as a result of metal−ligand dissociation under light irradiation. In contrast, a particularly appealing feature of iridium complexes that makes them unique is their larger d-orbital splitting, which leads to less-accessible metal-centered states that are likely capable of endowing the sensitizer with a better chemical stability to perform the utilization of solar energy in the long term.[13] More specifically, their strong σ-donation of the metalated carbon allows the MLCT state to be longer-lived and also tends to cause a decrease in the energy of the MLCT state via an enhancement of the ease of oxidation at the metal center.[14] All of these factors result in an improved absorption of visible light and help make these types of complexes well suited to operate as PSs for electron-transfer processes. However, this approach has thus far met with limited success, and only few iridium complexes with DSSC applications have been reported.[15] Yet, their potential as active materials associated with the conversion of light has received considerable attention.

As part of our recent investigation on iridium chemistry, we described the preparation of the iridium complex $[Ir(4\text{-}CF_3bt)_2(Hbpdc)]$ (**1**, where 4-CF_3bt = (4-trifluoromethyl)-2-phenylbenzothiazole and H_2bpdc = 2,2′-bipyridine-4,4′-dicarboxylate) in a preliminary report.[16] In this molecule, the 2-phenylbenzothiazole behaves as an attractive moiety in optoelectronic materials because of its extended π-conjugation length and its high chemical and photophysical stability in comparison with conventional phenylpyridine.[17] A trifluoromethyl group is incorporated onto the framework to impart greater electrophilicity at the metal center, which gives improved activities. N^N ligands bearing terminal carboxyl groups were included not only to increase the molar extinction coefficient and water solubility of the complex[18] but also to enable chemical grafting onto a TiO_2 support for the efficient and directional electron transport between the PS excited state and the conduction band of the TiO_2 semiconductor.[19] This complex displays an active photoinspired propensity for water splitting to produce hydrogen and for the clean photoconversion of CO_2. Several factors may be contributing to this behavior, including solvent effects, the pH of the reaction media, the concentration of PS, and the nature of the surrounding ligands. Encouraged by this finding, we decided to conduct detailed studies of iridium complexes with 2-phenylbenzothiazole and to study the influence of ligand modification on their chemical and other properties. Understanding the conformation and reactivity of such species is critical for achieving mechanistic insights into the active center

dx.doi.org/10.1021/ic202423y | Inorg. Chem. 2012, 51, 4123−4133

involved in photocatalysis and for developing new, selective catalysts for solar-light-driven, electron-transfer reactions. Here, we present the strategic design and synthesis of a series of heteroleptic iridium(III) compexes $[Ir(C^N)_2(Hbpdc)]$ **2**–**5** (where C^N = 2-phenylbenzothiazole and its derivatives), as depicted in Scheme 1. Variation of the ligand substitution to alter the electron densities in the ligand provides a means of tuning the orbital energetics and directly affects the electronic transitions of the resulting complexes for the thermodynamic driving forces required for electron transfer. By comparison with the hydrogen-production behavior of the known corresponding complex **1**, valuable information about the resulting structure–property relationships could potentially be deduced. The photovoltaic properties of DSSC with these newly developed sensitizers were evaluated to further extend the application of these complexes.

EXPERIMENTAL SECTION

General Experimental. All of the synthetic reactions for the complexes were performed under an atmosphere of dry nitrogen using standard vacuum line, Schlenk techniques. Workup and purification procedures were performed in air. The ligand 2,2′-bipyridine-4,4′-dicarboxylate (H_2bpdc) was prepared using procedures identical to those described previously.[20] The organic ligands 4-trifluoromethyl-2-phenylbenzothiazole (**L1**), 3-trifluoromethyl-2-phenylbenzothiazole (**L2**), 2-phenylbenzothiazole (**L3**), 2-phenyl-5-(trifluoromethyl)-benzothiazole (**L4**), and 2-(*N*,*N*-dimethyl-4-phenyl)-5-(trifluoromethyl)benzothiazole (**L5**) were prepared according to the general method.[21] The purification of the required final solid was accomplished by recrystallization from hot ethanol. The sensitized P25 was prepared using a slightly modified version of the published procedure, and the PS desorption process was similar to that used in our previous report.[16,22] Unless otherwise noted, all other chemicals were used as received without further purification. The anhydrous acetonitrile used for cyclic voltammetry measurements was supplied by Alfa Aesar. ^{1}H NMR spectra were recorded on a Bruker AMX-500 NMR spectrometer. The elemental analyses for C, H, and N were determined on a Perkin-Elmer 240C element analyzer. ESI mass spectra were obtained on a Thermo LCQ Fleet mass spectrometer. The absorbance measurements were performed using a Varian Cary 50 UV–vis spectrophotometer for solutions and a Shimadzu UV-2550 UV–visible spectrophotometer for solid samples. The fluorescence emission spectra were acquired with a Varian Cary Eclipse fluorescence spectrophotometer. Lifetime data were acquired with a Horiba Jobin-Yvon FluoroMax-4-TCSPC spectrometer. The electrochemical properties of the complexes in solution were investigated in a three-electrode cell consisting of a glassy carbon disk (3 mm diameter disk) working electrode, an auxiliary platinum wire, and an Ag/AgCl (saturated) reference electrode using a PARSTAT-2273 advanced electrochemical system. Single-crystal diffraction intensity data for complex **2** were collected at room temperature on a Bruker Smart CCD diffractometer equipped with a graphite-monochromated Mo Kα radiation (λ = 0.71073 Å) source. Single crystals of **3** and **4** were characterized on a CAD4/PC diffractometer using Mo Kα radiation (λ = 0.71073 Å). The structures were solved by the direct method and refined by the full-matrix least-squares method on all F^2 data using anisotropic thermal parameters for all non-hydrogen atoms.

General Synthetic Procedure for Iridium Complexes. The target complexes were prepared by a similar two-step bridge-splitting pathway.[16] A solution that contained the C^N ligand (2.2 mmol) and $IrCl_3{\cdot}H_2O$ (1.0 mmol) in a mixture of 2-ethoxyethanol (15 mL) and water (5 mL) was stirred at 140 °C for 24 h under nitrogen. After the mixture was cooled, the resulting precipitate was filtered and purified by silica-gel column chromatography with a mixture of EtOAc/hexane (1:4, v/v). The iridium dichloro-bridged dimer product was further recrystallized for the next step. Excessive Na_2CO_3 (10 mmol) was then added to the mixture of $Ir_2(C^N)_4Cl_2$ (0.3 mmol) and H_2bpdc (0.8 mmol) in CH_3OH/CH_2Cl_2 (30 mL, 1:1, v/v). The reaction mixture was heated at reflux for 24 h under nitrogen and cooled to room temperature, and the solvent was removed on a rotary evaporator under vacuum. The resulting solution was suspended by the addition of water and was acidified to a pH of approximately 5.0 with 0.5 M HCl solution. The crude product was obtained in a precipitate form and purified by column chromatography over silica gel (CH_3OH/CH_2Cl_2 as eluant, 1:1, v/v) followed by recrystallization to give the desired complex as an orange solid (yield: based on the starting dimer).

Ir(L2)$_2$(Hbpdc) (2). Yield 82%. ^{1}H NMR (500 MHz, CD_3COOD): δ 9.33 (2H, s), 8.40 (2H, s), 8.22 (4H, m), 8.10 (2H, J = 8.0 Hz, d), 7.49 (2H, m), 7.20–7.27 (4H, J = 8.5 Hz, d), 6.66 (2H, J = 6.5 Hz, d), 6.38 (2H, J = 6.5 Hz, d). Anal. Found for $C_{40}H_{21}F_6IrN_4O_4S_2$: C, 48.51; H, 2.12; N, 5.60. Calcd: C, 48.43; H, 2.13; N, 5.65. ESI MS (CH_3OH): 991.00 (m^+). Crystals of **2** that were suitable for X-ray diffraction were yielded at ambient temperature by slow diffusion of hexane into a saturated methanol solution of **2**.

Ir(L3)$_2$(Hbpdc) (3). Yield 85%. ^{1}H NMR (500 MHz, CD_3COOD): δ 9.29 (2H, s), 8.41 (2H, J = 8.5 Hz, d), 8.18 (2H, J = 6.5 Hz, d), 8.01 (2H, J = 8.0 Hz, d), 7.94 (2H, J = 6.5 Hz, d), 7.41 (2H, J = 6.5 Hz, t), 7.17 (4H, m), 6.94 (2H, J = 9.0 Hz, t), 6.48 (2H, J = 8.0 Hz, d), 6.33 (2H, J = 10 Hz, d). Anal. Found for $C_{38}H_{23}IrN_4O_4S_2$: C, 53.21; H, 2.82; N, 6.60. Calcd: C, 53.32; H, 2.71; N, 6.55. ESI MS (CH_3OH): 855.00 (m^+). Crystals of **3** that were suitable for X-ray crystal structure determination were obtained by the slow evaporation of a solution of **3** in methanol.

Ir(L4)$_2$(Hbpdc) (4). Yield 78%. ^{1}H NMR (500 MHz, CD_3COOD): δ 9.38 (2H, s), 8.57 (2H, J = 8.0 Hz, d), 8.29 (4H, m), 8.04 (2H, J = 6.5 Hz, d), 7.70 (2H, J = 8.0 Hz, d), 7.23 (2H, J = 8.5 Hz, t), 7.02 (2H, J = 6.5 Hz, t), 6.51 (2H, J = 6.0 Hz, d), 6.35 (2H, s). Anal. Found for $C_{40}H_{21}F_6IrN_4O_4S_2$: C, 48.51; H, 2.12; N, 5.60. Calcd: C, 48.43; H, 2.13; N, 5.65. ESI MS (CH_3OH): 990.67 (m^+). Crystals of **4** that were suitable for X-ray crystal structure determination were also grown by the slow evaporation of a methanol solution of **4**.

Ir(L5)$_2$(Hbpdc) (5). 2-Ethoxyethanol was used as a one-component solvent for the reaction of $Ir_2(C^N)_4Cl_2$ and H_2bpdc. Yield 78%. ^{1}H NMR (500 MHz, CD_3COOD): δ 9.35 (2H, s), 8.60 (2H, J = 8.0 Hz, d), 8.28 (2H, J = 5.5 Hz, d), 8.06 (2H, J = 6.5 Hz, d), 7.76 (2H, J = 8.0 Hz, d), 7.51 (2H, J = 8.5 Hz, t), 6.60 (2H, J = 6.5 Hz, d), 6.30 (2H, J = 6.0 Hz, d), 5.69 (2H, s), 2.70 (12H, s). Anal. Found for $C_{44}H_{31}F_6IrN_6O_4S_2$: C, 48.87; H, 2.96; N, 7.74. Calcd: C, 49.02; H, 2.90; N, 7.80. ESI MS (CH_3OH): 1076.67 (m^+).

Device Fabrication for DSSCs. The TiO_2 paste preparation and device fabrication for sandwich-type DSSCs were performed according to a previously reported procedure.[23] The practical TiO_2 photoelectrodes were soaked into a solution of the target complex (ca. 0.5 mM) in methanol for 24 h. After being washed with distilled water and dried at room temperature for 30 min, the resulting sensitized electrodes were assembled with a mirror-like sputtered-Pt counter electrode into a DSSC construction. The electrolyte used for all devices contained 1-butyl-3-methyl-imidazolium iodide (1.0 M), LiI (50 mM), I_2 (30 mM), and 4-*tert*-butylpyridine (0.5 M) in a mixture of acetonitrile and valeronitrile (v/v = 85:15). The current–voltage characteristics of the DSSCs were determined on a computer-controlled source-measurement unit (Keithley 236) under illumination from an AM 1.5G solar simulator (Oriel, model 92251A-1000) at 100 mW·cm^{-2}. The source-measurement unit was calibrated using a standard silicon reference cell (Oriel, model 91150 V).

Theoretical Calculations. All calculations were performed with the Gaussian 09 program based on the density functional theory (DFT) method. The geometric and energy optimizations of the complexes were performed with the use of B3LYP/LANL2DZ.[24] The numerical calculations in this paper were performed on the IBM Blade cluster system at the High Performance Computing Center (HPCC) of Nanjing University.

General Procedures of Photocatalytic Hydrogen Production. All H_2 production experiments were evaluated in a Pyrex vessel with a side visible-light irradiation using a 300 W xenon lamp equipped with a cutoff filter (radiation wavelength >420 nm), as described previously.[16] The reactor was charged with 10 μM of PS (or 0.1 g of

dx.doi.org/10.1021/ic202423y | Inorg. Chem. 2012, 51, 4123–4133

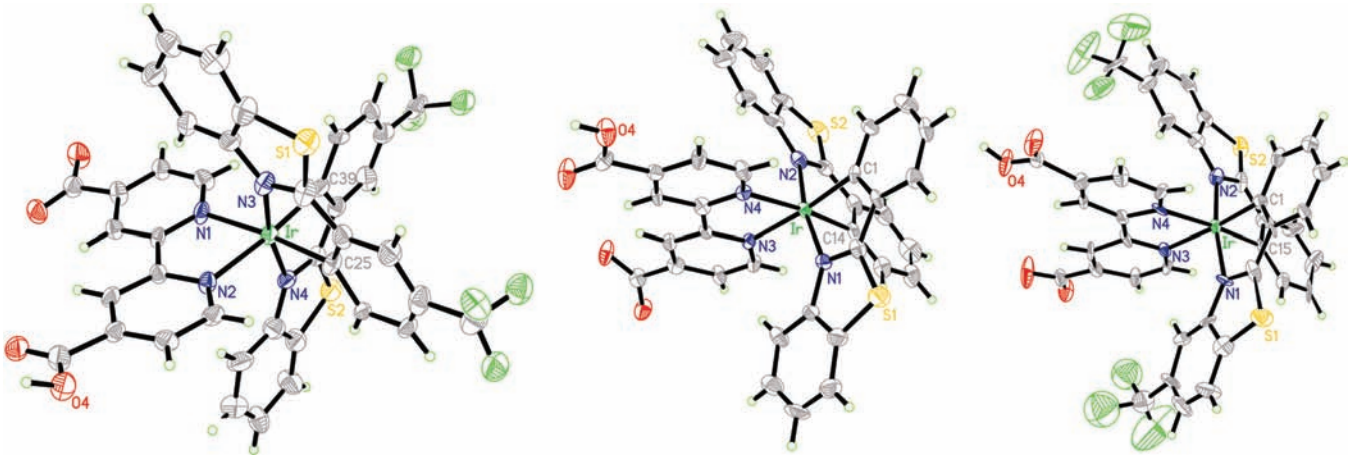

Figure 1. ORTEP drawings of complexes **2** (left), **3** (center), and **4** (right). The crystallographic data can be found in Supporting Information Tables S1−S4.

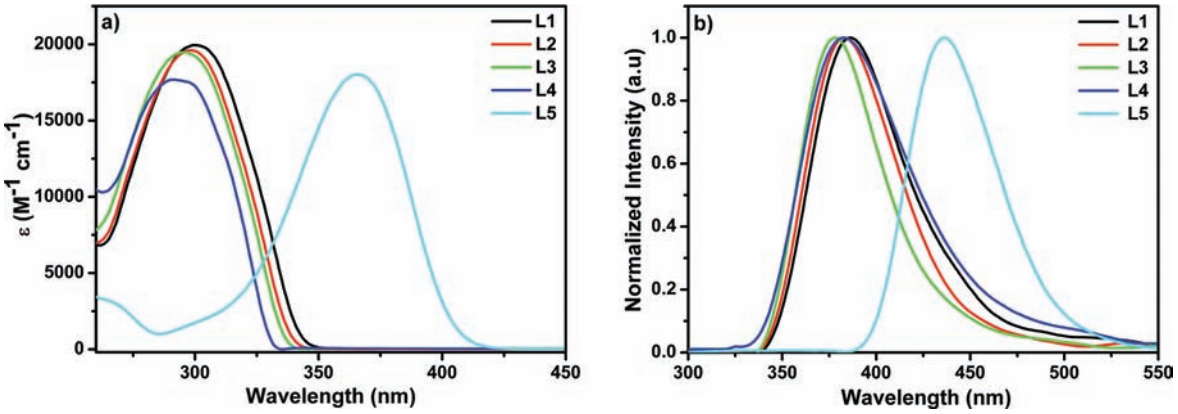

Figure 2. Electronic absorption spectra (a) and normalized photoluminescence spectra (b) of free ligands **L1**−**L5** in MeOH at 298 K.

PS-sensitized P25), 0.02 mM of catalyst (K_2PtCl_4), and 0.28 M of TEOA and was promoted with 0.14 M LiCl in an aqueous solution (270 mL) with gentle magnetic stirring (at neutral pH adjusted with concentrated hydrochloric acid). Prior to light irradiation, the system was evacuated successively before being backfilled with argon. The evolved gases were periodically detected in situ on a gas chromatograph equipped with a thermal conductivity detector (Shimadzu GC-8A).

RESULTS AND DISCUSSION

Synthesis and Characterization. The ring system of 2-phenylbenzothiazoles generated from the benzene attached at the C-2 position of benzothiazole, which shows efficient charge-transfer between these two functionalities, is similar to that of luciferin, which is famous for its surprising ability to produce chemiluminescence. Using lower-cost starting materials, a series of 2-phenylbenzothiazoles bearing substituents such as trifluoromethyl and *N*,*N*-dimethyl in the phenyl part and in the 5-position of the benzothiazole ring (Supporting Information Scheme S1) were easily obtained by condensation of commercially available 2-aminothiophenol and appropriate benzaldehydes in water in the presence of catalytic *p*-toluenesulfonic acid followed by recrystallization from ethanol on a multigram scale.[21] Attempts to prepare 2-trifluoromethyl-2-phenylbenzothiazole from 2-(trifluoromethyl)benzaldehyde in water or in $CHCl_3$ were unsuccessful, and no corresponding compound appeared in the reaction product even though a longer reaction time was used.

The synthesis of all of the target complexes takes advantage of a conventional reaction between the cyclometalated μ-chloride-bridged dimer $[Ir(C^N)_2Cl]_2$ and neutral H_2bpdc in the presence of Na_2CO_3. All of the emissive, mononuclear iridium(III) complexes were readily purified using column chromatography and were isolated in reasonably high yields. The structural identities of all complexes were fully identified by a combination of ^{1}H NMR, mass spectrometry, elemental analysis, and single-crystal X-ray crystallography for complexes **2**−**4**. The resulting products are stable in air and are partially soluble in CH_2Cl_2, $CHCl_3$, CH_3OH, and H_2O; the acquisition of good-quality ^{13}C NMR data was therefore difficult. The complexes failed to be converted into the corresponding cationic species as hexafluorophosphate salts by anion metathesis with NH_4PF_6 at room temperature. It is possible that the terminal deprotonated carboxyl group must satisfy the charge balance to meet the required stabilization for the $[Ir(C^N)_2]^+$ unit, as confirmed in the X-ray crystal structures of **1**−**4** (Figure 1). Thus far, research on metal iridium complexes such as $[Ir(C^N)_2(N^N)]^+$ has been focused on the polypyridyl N^N ligand, whereas less consideration has been given to those complexes that incorporate carboxylic-functionalized bipyridine-like ligands.[25]

The perspective views of the crystal structures of complexes **2**−**4** are shown in Figure 1. The crystal data and structure refinement for complexes **2**−**4** are listed in Supporting Information Table S1. In all cases, as well as in the case of

dx.doi.org/10.1021/ic202423y | *Inorg. Chem.* 2012, 51, 4123−4133

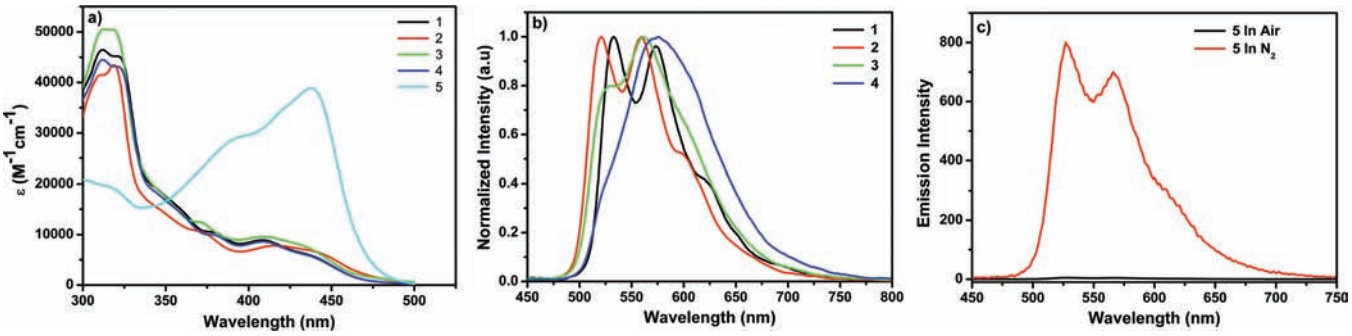

Figure 3. (a) Electronic absorption spectra of the complexes **1**−**5**. (b) Normalized emission spectra of the complexes **1**−**4** in air. (c) Photoluminescence emission spectra for complex **5** under a difference atmosphere of nitrogen and air. Spectra were taken in MeOH at ambient temperature. The spectra for the known complex **1** are also shown for comparison.

Table 1. Photophysical and Electrochemical Properties of Complexes 1−5 at Room Temperature

complex	λ_{em} (nm)[a]	τ (ns)[a]	E_{ox} (V)[b]	E_{red} (V)[b]	ΔE (V)	E_{0-0} (eV)[c]	$E(S^+/S^*)$[d]
1	536, 572	114	+1.22	−1.26	2.48	2.42	−1.20
2	520, 558	146	+1.24	−1.03	2.27	2.40	−1.16
3	528(sh), 560	99	+1.20	−1.06	2.26	2.38	−1.18
4	574	118	+1.22	−1.52	2.74	2.42	−1.20
5	527, 566[e]	*f*	+1.18	−1.29	2.47	2.39	−1.21

[a]Measured in air-equilibrated MeOH; the symbol "sh" denotes the shoulder wavelength. [b]Redox measurements were performed in deoxygenated anhydrous MeCN (for **5**, in DMF) with $^nBu_4NPF_6$ (0.1 M) relative to Ag/AgCl used as reference electrode (calibrated with Fc/Fc^+ prior to each experiment); the potential was adjusted with respect to the normal hydrogen electrode (+197 mV vs NHE); scan rate 50 mV s^{-1}. For both **2** and **3** only the first reduction is shown. [c]The E_{0-0} energy was estimated from the onset of the absorption spectrum in MeOH. [d]$E(S^+/S^*) = E_{ox} - E_{0-0}$. [e]Measured in nitrogen-saturated MeOH. [f]Not determined owing to no luminescence observed in air-equilibrated MeOH.

the previously reported complex **1**,[16] each iridium atom is hexacoordinated by the carbon and nitrogen atoms of two cyclometalating C^N ligands and the nitrogen atoms of the Hbpdc N^N ligand. An examination of the metal−ligand bonds revealed that the Ir−C distances of these complexes are significantly shorter than the Ir−N distances, which is consistent with the bond lengths observed in similar $[Ir(C^N)_2(N^N)]^+$ complexes.[26] The associated Ir−N distances vary from 2.104 to 2.163 Å for Ir−N(Hbpdc) and from 2.044 to 2.089 Å between the Ir center and the nitrogen atom of the cyclometalated ligand, which may be caused by a stronger metal−ligand interaction with the cationic Ir(III) ion. As might be expected, the average Ir−C distance in complex **3** (2.016 Å) was found to be significantly shorter than those observed in both **1** (2.020 Å) and **2** (2.019 Å). The longer Ir−C distances in complexes **1** and **2** are attributed to the presence of a highly electron-withdrawing substituent on the phenyl ring of the C^N ligand, which reduces the donating ability to the metal and then weakens the Ir−C covalent bond, thereby giving rise to a slight lengthening in comparison to the Ir−C distance in **3**. Accordingly, these observed effects are favorable for achieving a better understanding of the underlying chemical and photophysical properties of these complexes.

Photophysical Properties. Absorption and emission spectra were recorded in methanol for all C^N ligands, as shown in Figure 2. Each of the electronic absorption properties of the ligands **L1**−**L4** is dominated by a broad absorption band at 290−300 nm, which arises from intraligand charge-transfer (ILCT) transitions that possibly involve phenyl-to-benzothiazole charge transfer. Compared with those of **L3**, the absorption spectra of the ligands **L1**, **L2**, and **L4** exhibit a small shift of ca. 10 nm due to the effect of the electron-withdrawing trifluoromethyl substituent, and the presence of this substituent leads to an energetic change in the optical transitions. When the CF_3 group is located on the phenyl moiety in **L1** and **L2**, it causes a red-shift; however, when located at the 5-position of the benzothiazole ring in **L4**, it leads to a blue-shift. For **L5**, which features an intramolecular donor−acceptor (DA) system, the collective effect of both the electron-donating *N*,*N*-dimethyl group on the phenyl moiety and the electron-withdrawing trifluoromethyl group at the 5-position of the benzothiazole ring is considered to enhance the DA character and to therefore induce a significant red-shift of the absorption band (367 nm) relative to those of **L1**−**L4**.

Because of the effect of coordination to the metallic center, all the complexes except **5** exhibit intense absorption bands in the 300−330 nm range and weak absorption bands centered at ca. 408 nm (except for that of **2**, which is centered at 415 nm) with the tail extending well into the visible region, as shown in the patterns in Figure 3a. These results imply that the chromophores remain nearly unperturbed by the presence of different substituents installed on the C^N ligand, at least with respect to the absorption properties. In accordance with previous studies on related bis-cyclometalated iridium(III) diimine complexes, the intense absorption can generally be associated with spin-allowed ligand-centered (LC) $\pi \rightarrow \pi^*$ transitions centered on both the N^N and C^N ligands, whereas the weak, broad absorption bands at low energy have been ascribed to both metal-to-ligand charge-transfer (MLCT) and ligand-to-ligand charge-transfer (LLCT) transitions.[24,27] Finally, the absorption tail ($\lambda > 450$ nm) can be explained by a convolution of spin-forbidden CT transitions due to the induction of strong spin−orbit coupling by Ir(III). A careful comparison of the absorption onset in their absorption spectra reveals only slight differences with almost negligible shifts, which suggests that the incorporation of a CF_3 group has very little effect on the lowest excited state of **1**−**4**.[28] Unlike the absorption spectra of complexes **1**−**4**, however, the spectrum of

dx.doi.org/10.1021/ic202423y | Inorg. Chem. 2012, 51, 4123−4133

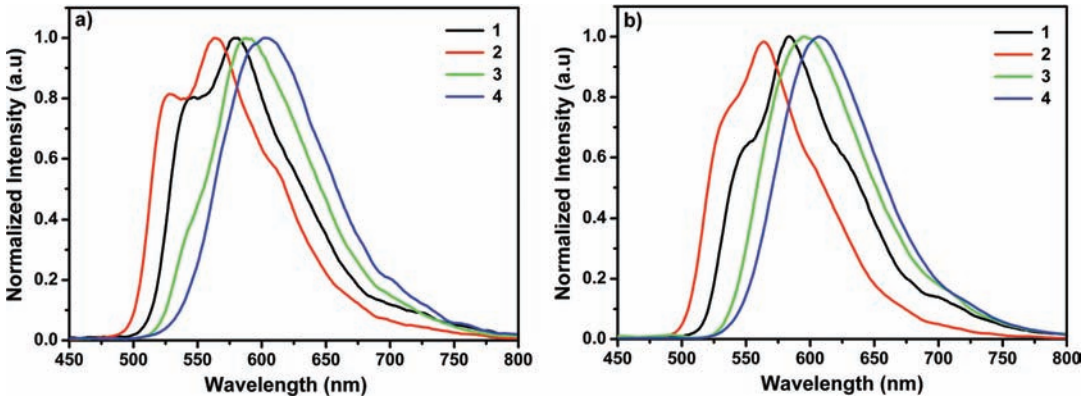

Figure 4. Normalized fluorescence spectra of complexes **1**−**4** recorded in neat thin films (a) and as solid powders (b).

5 displays a particularly intense absorption band (438 nm) with a shoulder, which is presumed to arise from an IL transition on the C^N ligand probably mixing to a certain degree with the character of the LLCT transition from the π orbital of the amino-substituted C^N to the π^* orbital of the N^N moiety. With respect to the typical absorption profiles of the complexes, they provide the possibility of receiving light across a wide spectral range, which is a favorable characteristic for their potential application in solar-to-energy conversion. In addition, the modification of the C^N ligand thus facilitates wavelength variation in the emission spectra of the corresponding complexes.

With respect to the emission spectra collected in ambient air at room temperature, complexes **1**−**4** all exhibited structured emissions with wavelengths of the first peak or shoulder at approximately 520−532 nm in methanol (Figure 3b). These emissions are due to the presence of an excited state derived from the mixing of the ^{3}MLCT and ^{3}LC states. These emissive complexes exhibit Stokes shifts that are sufficiently large to minimize the spectral emission overlap with the lowest-energy MLCT absorption bands because of the weak oscillator strength of the ^{3}MLCT, which is indicative of phosphorescence.[29] In addition, the excited-state lifetime of **2** is longer than that of complexes **1**, **3**, and **4** in air-equilibrated methanol solution, as detailed in Table 1. However, compared to complexes **1**−**4**, complex **5** is practically nonemissive in air-saturated methanol at room temperature, possibly because of the presence of the dimethylamino group. The lack of emission from **5** indicates that it is susceptible to oxygen quenching, which has been commonly observed in Ru(II) and Pt(II) complexes but in very few of the Ir(III) complexes used for the oxygen sensing.[30] As clearly shown in Figure 3c, this inefficient emission can be remarkable enhanced in oxygen-free methanol. This photoluminescence emission may arise from ^{3}IL rather than ^{3}MLCT emissive states of general iridium(III) complexes.

To investigate their potential use as host phosphors, solid-state emission spectra of **1**−**4** were collected for samples prepared as thin films and as solid powders (Figure 4). A comparison of emission intensity is presented in Supporting Information Figures S13 and S14. Upon photoexcitation, complexes **1**−**4** display poorly structured, broad spectra with obvious red-shift effects compared with the spectra collected from solution-based samples, and their emission colors range from orange to red. The red shift and long tails in both solid-state emission spectra are related to strong intermolecular π−π stacking between the adjacent chromophores; such packing has been observed in the crystal structures of **1**−**4**. Figure 4 reveals that the photophysical properties as well as the previously discussed structural aspects are sensitive to the position of the trifluoromethyl substituent in **1** and **2**, which effectively stabilizes the HOMO energy level by easing electron density from the metal, which increases the energy gap; this stabilization occurs when the trifluoromethyl substituent is in either the *meta* or *para* position relative to the coordination site in the complexes. As a result, the complexes exhibit the expected blue-shifted emission relative to the unsubstituted complex **3**. Conversely, a comparison of **4** with the parent **3** reveals that the introduction of the inductively CF_3 group into the 5-position of the electron-deficient benzothiazole ring leads to a red-shift of 15 nm, which is mostly due to the increased intramolecular DA interaction. In addition, the emission spectra of complexes **1**−**5** were also examined after the complexes were cast into a rigid medium—poly(methyl methacrylate) (PMMA) (see Supporting Information Figures S15 and S16). The resulting emission spectra for **1**−**4** are similar to those obtained in methanol-based media, which suggests that the transparent PMMA supporting matrix has the ability to stabilize the charge-transfer excited state.[31] Notably, the blending with PMMA seems to be highly beneficial for the photoluminescence of complex **5** because the emission intensity in the matrix increases significantly, which is attributed to a reduction of the self-quenching from intermolecular interactions.

Electrochemical Properties. To qualitatively estimate the frontier molecular orbitals, particularly the HOMO energy levels based on the ionization potential for the first oxidation, cyclic voltammetry experiments were undertaken in MeCN (apart from that for **5**, which was performed in DMF) in terms of the solubility of the complexes. The electrochemical data are listed in Table 1. An oxidation occurred at a similar potential between 1.18 and 1.24 V versus NHE for all complexes. The oxidation is likely associated with a one-electron Ir(III)/Ir(IV) oxidation process,[32] i.e., the removal of an electron from the metal-centered ground state. The higher oxidation potentials observed for **1**, **2**, and **4** are due to the lower electron densities on the metal center, which are primarily caused by the electronic effect of the CF_3 substituent. This electronic effect consequently makes the metal oxidation more difficult. The electron-withdrawing effect of the CF_3 group increases the electrochemical gap from 2.26 V in **3** to 2.74 V in **4**, which gives an initial estimate for the qualitative difference in the energy stored in the excited states (see also the computational results). The results suggest that the CF_3 group is effective in helping the HOMO become stabilized and also imparts a marked effect

dx.doi.org/10.1021/ic202423y | *Inorg. Chem.* 2012, 51, 4123−4133

Table 2. Spatial Plot of HOMO and LUMO Distributions for Complexes 1−5

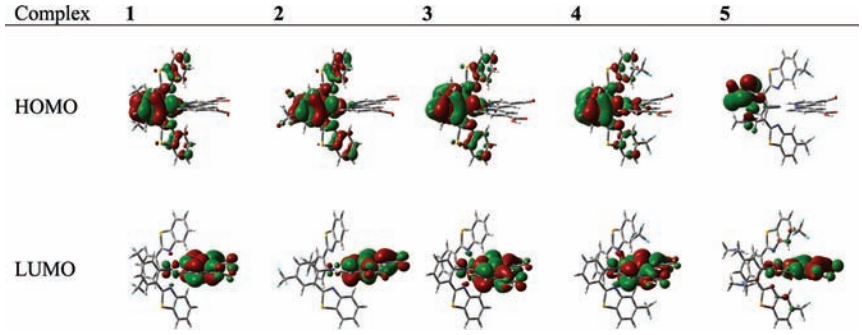

on the LUMO for this series of iridium complexes. As anticipated, the opposite effect is clearly observed in the presence of the electron-donating dimethylamino (NMe_2) group on the phenyl ring of the chromophoric C^N ligand. In addition, the cyclic voltammograms display a reduction wave with potentials that range from −1.03 to −1.52 V. In contrast with the oxidation process, the reduction may occur on the low-lying π^* orbitals that involve the surrounding chelates together with only a minor contribution from the metal center, that is, the addition of an electron to the ligand-centered LUMO. The potential difference between two redox waves reflects a ^{1}MLCT electronic transition and can be directly assigned to the emitted radiant energy of the complex. For **2** and **3**, the additional reduction of the C^N rings occurs at a more negative potential. The absence of the second reduction wave in the CV remained normal in the unfluorinated parent iridium complexes.

To gain fundamental insight into the electrochemical and photophysical behaviors of all the investigated complexes, molecular orbital (MO) calculations were performed at the density functional theory (DFT) level (see Table 2). In this regard, comparisons of the relative energies and compositions of the MOs with the nature of the electronic transitions involved in each absorption and emission band for the complexes are useful. The optimized structures of complexes **2**−**4** are in close agreement with the corresponding experimental values obtained from the X-ray crystallographic studies. The orbital compositions of the HOMOs and LUMOs in **1**−**4** are, in general, the same. The HOMOs consist of a mixture of Ir d_π and π orbitals of the whole conjugated C^N planes, whereas a small change in **4** is found to result from the HOMO mixing with a small region of the $\pi_{N^\wedge N}$ orbital. Conversely, the LUMOs for these four complexes primarily reside on the ancillary N^N π^* orbital mixed with very minor contributions from the d orbitals of the Ir and C^N ligands. This mixing explains the small effect of C^N on the potential of the N^N-based redox wave, except in the case of **2**. In addition, the participation of the central metal ion promotes the electron-transfer reductive reactions and causes an increased spatial separation of the charges in the excited state. On the basis of the DFT calculations, the electronic transition in the low-energy regions in **1**−**4** is mainly attributed to the ^{3}MLCT [$d\pi$(Ir) → $\pi^*_{N^\wedge N}$] and/or ^{3}LLCT ($\pi_{N^\wedge C}$ → $\pi^*_{N^\wedge N}$) transitions.

Although there is no apparent contribution from the CF_3 group to the HOMO character, which supports the experimental CV results, as detailed in Table 2, the nature of the substituent does appear to affect the overall energy level. This effect is especially evident in the case of the location of the HOMO differing with the site of the CF_3 group on the metalated C^N ligand. As previously stated, a dramatically blue-shifted emission in these systems can be achieved in both heavy complexes **1** and **2**, in which the electron-withdrawing effect stabilizes the HOMO to a greater extent than the LUMO compared to the stabilization observed in complex **3**. The stabilization of the HOMO leads to an increase in the HOMO−LUMO energy gap, which results in a blue-shift. The DFT calculations indicate that complex **2** with an electron-withdrawing group located in the *para* position relative to the coordination site exhibits the largest HOMO−LUMO gap and will therefore exhibit the most strongly blue-shifted emission among these complexes, as observed in the photoluminescent and electrochemical results. In addition, the relative stabilizations justify the higher oxidation potential measured for complexes **1** and **4**. The rough HOMO−LUMO energy gap increases by 0.21 and 0.44 eV in passing from **1** and **4** to **3**, respectively, which is consistent with the increased electrochemical $E_{ox} - E_{red}$ gap (0.22 and 0.48 V, respectively).

Regarding complex **5**, the HOMO is almost exclusively distributed on the $N(CH_3)_2$ fragments and on the adjacent phenyl group of the C^N ligands, with no electron density located on the Ir center; the HOMO, therefore, shows no overlap with the LUMO, as seen in the results in Table 2. The electron-donating NMe_2 group exerts a strong electron-donating effect on the phenyl units, increases the π-orbital energy of the moiety, and leads to an elevation of the HOMO levels relative to those in its counterpart **4**. Overall, a smaller band gap is obtained for **5**. The results also clearly reflect that the lowest transition of **5** is dominated primarily by ^{3}LLCT rather than ^{3}MLCT states.

The experimental and computational data suggest that the optical characteristics can feasibly be tuned through the appropriate functionalization of the cyclometalated ligand within the corresponding complexes without significant regard for the interplay between the HOMO and LUMO states. Equally important, the excited-state oxidation potential $E(S^+/S^*)$ for **2**−**5** is similar to that for **1**, which, as estimated from the oxidation potential and the optical absorption, is between −1.16 and −1.21 V versus NHE. The level is sufficiently more negative than the redox potential of H^+/H_2 (−0.41 V vs NHE, pH 7), which provides a sufficient driving force for H_2 production from water.[33] The excited state of complex **2** exhibits a particularly strong reducing strength; it can therefore be concluded that **2** will be more effective for photocatalytic hydrogen production. The potentials of the species are correctly placed for efficient electron transfer relative to the conduction-band edge of TiO_2 (ca. −0.5 V vs NHE at pH 7) and to an electrolyte that contains the I^-/I_3^- redox couple (ca. 0.4 V vs NHE), which shows that the prerequisite for further DSSC applications has been fulfilled.

dx.doi.org/10.1021/ic202423y | Inorg. Chem. 2012, 51, 4123−4133

Hydrogen Production. In our previously studies, complex **1** functioned as a PS in a light-driven system for the photogeneration of H_2 from water upon visible-light irradiation (λ > 420 nm).[16] As an extension of our previous work, the photoinduced reaction activities of these complexes were initially evaluated to investigate the impact of ligand modification on the PS performance of hydrogen evolution. Hydrogen-production experiments were performed to compare the effectiveness of **2**−**5** with that of **1** under identical conditions. All other conditions in the photocatalytic processes were kept constant (including the concentration) to ensure that comparisons between the complexes were meaningful. A typical three-component hydrogen-evolving system contained complex **2**−**5** (10 μM), a colloidal platinum catalyst (0.02 mM), and TEOA, which acted as a sacrificial electron donor, in 270 mL of neutral water (the free PS content was 2.7 μmol to allow a fair comparison with the bound systems; see below). The systems were irradiated under a 300 W xenon lamp equipped with a cutoff filter (λ > 420 nm). The evolution of hydrogen gases was monitored in situ periodically using an online gas chromatograph. The effectivity toward light-driven hydrogen production in water with different complexes is given in Figure 5. No

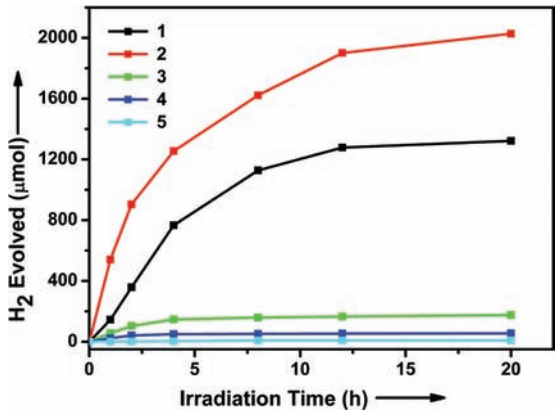

Figure 5. Photoinduced hydrogen evolution of **1**−**5** (10 μM) with *in situ* generated colloidal Pt (0.02 mM) in aqueous solution at pH 7.0 (λ > 420 nm). The data for **1** was taken from our previous report.

appreciable H_2 formation was observed in the absence of either light, PS, platinum catalyst, or TEOA in the mixture. Reductive quenching of the excited state by TEOA was observed with a linear Stern−Volmer plot for **1**−**4**. Complex **1** therefore allows for efficient quenching, but the quenching of **2**−**4** was less efficient (Supporting Information Figure S17).[16] The preliminary studies reveal that hydrogen can be successfully generated from water in the presence of catalytic amounts of platinum with all complexes. The introduction of the carboxyl group not only enables an increased tolerance of water but also ensures a good electronic communication between the excited chromophore and the Pt catalytic center. Notably, this work was performed on a 270 mL scale and demonstrated that this reaction has the potential for the production of a significant quantity of hydrogen. As evident from the results, both **1** and **2** give better results, and **2** exhibits a maximum amount of H_2 production (2027 μmol) with total turnover numbers (TONs) of 1501 after 20 h of illumination time. The performance of **2** is attributed to the significant reducing power of the complex's excited state. This value is significantly greater than that for **1** and also greater than the values of most of molecular systems for photodriven H_2 production in neutral water.[7] The results suggest that the position of the electron-withdrawing substituent has an obvious influence on the photoelectron transfer and thus also influences the activity. When using **3**, **4**, and **5** as the PS, the yield decreases significantly relative to those achieved with complexes **1** and **2**; these complexes may destabilize an additional charge-separation state of the photoinduced process. The total amount of H_2 for complexes **3**, **4**, and **5** was 175, 55, and 9 μmol with the TONs of 130, 41, and 7, respectively. As would be expected, hydrogen generation commences following the order as the activity of **2** > **1** > **3** > **4** as a result of the electronic effect from the attachment of CF_3 groups. In addition, the powerful reductive quencher of TEOA for **1** and the long lifetime of complex **2** correlate with the observed increased performance in the catalytic system (Supporting Information Figures S17 and S18). Although complex **5** exhibits a fairly intense absorption in the visible region, it is not active; we ascribe this result to the nature of the electron transitions in the low-energy region. In **5**, the absorption prefers a predominance of LLCT intraligand bands that lack the directionality of MLCT bands, which limits the ability of **5** to promote effective charge separation as a PS.

To investigate the role of carboxylated linkages in the complexes, **2**−**5** were grafted onto commercial nanoparticulate TiO_2 (Degussa P25) for visible-light absorption. Because their energy levels ensure electron injection from the photoexcited state into the TiO_2 conduction band (CB), additional activity in the production of hydrogen by the heterogeneous systems was expected.[34] In the presence of K_2PtCl_4 and TEOA, visible light-driven H_2 production by sensitized P25 using **2**−**5** is shown in Table 3 and compared to that of **1**. The observed TONs of

Table 3. Visible Light-Induced H_2 Evolution with PS Sensitized P25 in TEOA Buffer[a]

sample	adsorption on P25[b] (μmol/0.1 g)	H_2 (μmol)	TON[c]
1/P25	2.65	1621	1223
2/P25	2.17	1253	1155
3/P25	3.01	403	268
4/P25	2.56	131	102
5/P25	3.34	512	307

[a]All systems contained 0.1 g of sensitized TiO_2, 0.02 mM K_2PtCl_4, 0.28 M TEOA, and 0.14 M LiCl in 270 mL of aqueous solution under continuous irradiation with visible light (Xe-lamp with a cutoff filter, λ > 420 nm). The pH was adjusted to neutral by the addition of concentrated HCl. [b]The total amount of complexes **1**−**5** attached on P25 was determined after desorption from a methanol solution of NaOH at room temperature. [c]TON = $2n(H_2)/n$(PS).

hydrogen production for the TiO_2-anchored samples are significantly higher, except for that of **2**, when compared to the unattached homogeneous systems under similar conditions. The total amount of complexes **1**−**5** attached on P25 was determined after desorption from a methanol NaOH solution at room temperature (Table 3), which suggests that the loading of PS into the bound systems approximately matches that in the 10 μM homogeneous systems, except in the case of **2**. Notably, sensitized TiO_2 has a positive effect on the hydrogen production of these heterogeneous systems based on P25 sensitized with **3**−**5**. The performance for **5**-P25, in particular, is dramatically better (entry 5); its TON increased to a greater degree than that achieved with unbound chromophore **5** (TON, from 7 to 307), mainly due to the intense absorption in

dx.doi.org/10.1021/ic202423y | *Inorg. Chem.* 2012, 51, 4123−4133

the visible region. The charge transfers at the TiO_2/PS interfaces were also investigated to demonstrate the application of these assemblies in DSSCs.

Photovoltaic Properties. With a better understanding of the previously discussed electrochemical and photophysical properties, dye-sensitized solar cells were prepared using complexes **1**–**5**, and the photovoltaic performance of these solar cells was measured under AM 1.5G conditions (100 mW/cm^2). The results are shown in Figure 6, and detailed device parameters are provided in Table 4. The measurement delay time of the photo I–V characteristics of the DSSCs was fixed at 50 ms. The results clearly imply that all of the complexes **1**–**5** work properly for harvesting light in the cell and that the injected electrons are transported to generate electricity. However, their energy-to-electricity capabilities are relatively low and are not comparable with those of the art ruthenium dyes, such as N719. This low performance is primarily due both to the relatively low optical absorbance of these iridium complexes and to the low level of adsorption on the TiO_2 surface.

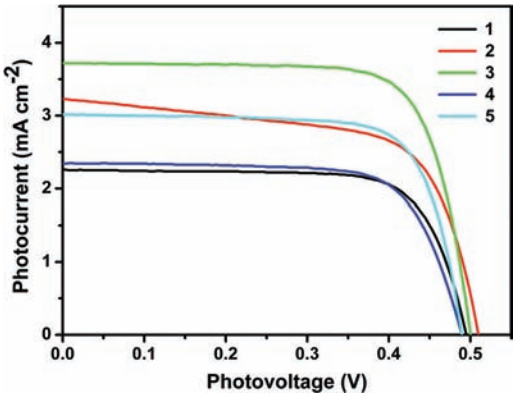

Figure 6. Photocurrent density–voltage (J–V) characteristic curves for DSSC devices containing **1**–**5** as PSs recorded under illumination of simulated solar light (AM 1.5G, 100 mW/cm^2).

Table 4. Detailed Photovoltaic Data of DSSCs Based on 1–5[a]

PS	V_{oc} (V)	J_{sc} (mA/cm^2)	FF	η (%)	adsorption[b] (10^{-7} mol/cm^2)
1	0.495	2.258	0.73	0.82	0.628
2	0.510	2.227	0.72	0.76	0.951
3	0.500	3.720	0.74	1.39	0.721
4	0.490	2.348	0.72	0.82	0.681
5	0.489	3.015	0.74	1.09	0.499

[a]Under standard AM 1.5G spectral conditions and at 100 mW/cm^2 light intensity; V_{oc}, open-circuit photovoltage; J_{sc}, shot-circuit photocurrent density; FF, fill factor; η, power conversion efficiency. [b]The total adsorption amount per unit area of TiO_2 film was estimated after desorption from a methanol solution of NaOH at room temperature.

The open-circuit voltages (V_{oc}) are similar for all five devices based on complexes **1**–**5**. The V_{oc} values are related to both the position of the Fermi level of TiO_2 and the redox potential of the electrolyte. The fill-factor (FF) values are nearly constant (0.72–0.74), which indicates similar device configurations. The short-circuit current density (J_{sc}) follows in the order **3** > **5** > **4** > **1** > **2**, which produces better performance in devices that contain **3** and **5** as the PS than in those that contain **1**, **2**, or **4**. The DSCC achieves an energy conversion efficiency (η) of 1.39% with complex **3**, which is the highest among the five cells studied in this work under the same cell fabrication and efficiency-measurement procedures. For comparison, a cell was fabricated with the art ruthenium dye N719 under the same conditions, which gave a η value of 7.8% (Supporting Information Figure S25). The relatively high J_{sc} value for the device may also arise from the relatively higher HOMO level of **3** relative to that of other complexes except for **5**, and this higher HOMO level may permit a more facile regeneration to the oxidized dye. In contrast, the J_{sc} values are clearly poor in the devices that contain **1**, **2**, and **4**. These results reveal the effect of the incorporation of a strong electron-withdrawing CF_3 unit into the PS system, which reduces the desired electron transfer from the excited PS molecular to the TiO_2 conduction band. In addition, the enhancement in the J_{sc} of **5** is attributed to its optical-absorption profile. The molecular size (and therefore the quantity of PS molecules loaded onto a TiO_2 electrode) of the PS also affects the current density and thus the performance of the DSSC.[35] Although complex **5** exhibits an outstanding photoresponse relative to that of complex **3**, complex **5** produced lower J_{sc} values, which is partially due to a smaller amount of **5** being molecularly adsorbed onto TiO_2 relative to the amount of adsorbed **3**.

CONCLUSIONS

A series of heteroleptic cyclometalated iridium(III) complexes, in cooperation with phenylbenzothiazole and bipyridine dicarboxylate, which were used during experiments that addressed the desirable and tunable photophysical characteristics, have been newly synthesized in an attempt to identify the connection between their structure and function. With the aid of theoretical calculations, the spectroscopic and electrochemical behaviors as they pertain to the light absorption and electron-transfer processes of the complexes were elucidated. These complexes are suitable for solar-energy conversion applications, such as photoinduced hydrogen production and dye-sensitized solar cells. The structural modification of the cyclometalated ligand around the metal appears to be beneficial to the photohydrogen-evolution activity. In particular, the electronic effects of the inductively electron-withdrawing CF_3 moiety enable complexes **2** to exhibit a maximum hydrogen production with the total TON of 1501 from the neutral water. In addition, after the complexes were used in conjunction with TiO_2 (P25) nanoparticles for the fabrication of heterogeneous photocatalytic systems, a clear change in their activity behaviors was observed as a result of the induction of efficient charge separation. The photovoltaic performances of solar cells sensitized with these five iridium complexes were also investigated under full sun. With a particular donor group, such as NMe_2, introduced into the chromophoric C^N ligand, as in complex **5**, an apparent enhancement of the molar extinction coefficient was induced for the lowest energy band, which increased its visible-light-harvesting capacity. As it stands, these investigations on the structure–activity relationships allow us to better understand photoassisted electron transfer to redox-active trap sites and may also stimulate the development of these encouraging light-harvesting complexes for promising solar-to-energy conversion.

dx.doi.org/10.1021/ic202423y | Inorg. Chem. 2012, 51, 4123–4133

■ ASSOCIATED CONTENT

Supporting Information

X-ray crystallographic data of complexes **2**−**4** in CIF format, solid-state absorption and emission spectra for complexes **1**−**5**, emission decay kinetics for complexes **1**−**4**, Stern−Volmer plot for emission quenching of complexes **2**−**4** by TEOA, dark current−voltage curves of the DSSCs based on sensitizers **1**−**5**, photocurrent−voltage (*J*−*V*) characteristics for DSSC based on N719 dye, tables of the crystallographic data for complexes **2**−**4**, and ^{1}H NMR and MS spectra and CV data for all new complexes in this work. This material is available free of charge via the Internet at http://pubs.acs.org.

■ AUTHOR INFORMATION

Corresponding Author

*E-mail: yuzt@nju.edu.cn; zgzou@nju.edu.cn.

Notes

The authors declare no competing financial interest.

■ ACKNOWLEDGMENTS

This work was financially supported by the National Science Foundation of China (Grant No. 20901038) and the Fundamental Research Funds for the Central Universities (Grant Nos. 1106021342 and 1117021302). We are also grateful to the Scientific Research Foundation for the Returned Overseas Chinese Scholars, State Education Ministry.

■ REFERENCES

(1) (a) Lewis, N. S.; Nocera, D. G. *Proc. Natl. Acad. Sci. U.S.A.* **2006**, *103*, 15729−15735. (b) Tollefson, J. *Nature* **2010**, *464*, 1262−1264. (c) Eisenberg, R.; Nocera, D. G. *Inorg. Chem.* **2005**, *44*, 6799−6801. (d) Karunadasa, H. I.; Chang, C. J.; Long, J. *Nature* **2010**, *464*, 1329−1333. (e) Armaroli, N.; Balzani, V. *Angew. Chem., Int. Ed.* **2007**, *46*, 52−66.

(2) (a) Barber, J. *Chem. Soc. Rev.* **2009**, *38*, 185−196. (b) Morris, A. J.; Meyer, G. J.; Fujita, E. *Acc. Chem. Res.* **2009**, *42*, 1983−1994. (c) Walter, M. G.; Warren, E. L.; McKone, J. R.; Boettcher, S. W.; Mi, Q. X.; Santori, E. A.; Lewis, N. S. *Chem. Rev.* **2010**, *110*, 6446−6473. (d) Krassen, H.; Ott, S.; Heberle, J. *Phys. Chem. Chem. Phys.* **2011**, *13*, 47−57.

(3) (a) Zhang, J.; Du, P.; Schneider, J.; Jarosz, P.; Eisenberg, R. *J. Am. Chem. Soc.* **2007**, *129*, 7726−7727. (b) White, T. A.; Whitaker, B. N.; Brewer, K. J. *J. Am. Chem. Soc.* **2011**, *133*, 15332−15334. (c) Reisner, E.; Powell, D. J.; Cavazza, C.; Fontecilla-Camps, J. C.; Armstrong, F. A. *J. Am. Chem. Soc.* **2009**, *131*, 18457−18466. (d) Youngblood, W. J.; Lee, S. H. A.; Kobayashi, Y.; Hernandez-Pagan, E. A.; Hoertz, P. G.; Moore, T. A.; Gust, D.; Mallouk, T. E. *J. Am. Chem. Soc.* **2009**, *131*, 926−927.

(4) (a) Hirata, N.; Lagref, J. J.; Palomares, E. J.; Durrant, J. R.; Nazeeruddin, M. K.; Grätzel, M.; Censo, D. D. *Chem.—Eur. J.* **2004**, *10*, 595−602. (b) Fihri, A.; Artero, V.; Razavet, M.; Baffert, C.; Leibl, W.; Fontecave, M. *Angew. Chem., Int. Ed.* **2008**, *47*, 564−567. (c) Utschig, L. M.; Silver, S. C.; Mulfort, K. L.; Tiede, D. M. *J. Am. Chem. Soc.* **2011**, *133*, 16334−16337.

(5) (a) Du, P.; Schneider, J.; Jarosz, P.; Eisenberg, R. *J. Am. Chem. Soc.* **2006**, *128*, 7726−7727. (b) Zhang, P.; Wang, M.; Na, Y.; Li, X.; Jiang, Y.; Sun, L. C. *Dalton Trans.* **2010**, *39*, 1204−1206. (c) Dempsey, J. L.; Winkler, J. R.; Gray, H. B. *J. Am. Chem. Soc.* **2010**, *132*, 16774−16776. (d) Elvington, M.; Brown, J.; Arachchige, S. M.; Brewer, K. J. *J. Am. Chem. Soc.* **2007**, *129*, 10644−10645.

(6) (a) Gärtner, F.; Sundararaju, B.; Surkus, A. E.; Boddien, A.; Loges, B.; Junge, H.; Dixneuf, P. H.; Beller, M. *Angew. Chem., Int. Ed.* **2009**, *48*, 9962−9965. (b) Rau, S.; Schäfer, B.; Gleich, D.; Anders, E.; Rudolph, M.; Friedrich, M.; Görls, H.; Henry, W.; Vos, J. G. *Angew. Chem., Int. Ed.* **2006**, *45*, 6215−6218. (c) Karnahl, M.; Kuhnt, C.; Ma, F.; Yartsev, A.; Schmitt, M.; Dietzek, B.; Rau, S.; Popp, J. *ChemPhysChem* **2011**, *12*, 2101−2109.

(7) (a) Jiang, D. L.; Choi, C. K.; Honda, K.; Li, W. S.; Yuzawa, T.; Aida, T. *J. Am. Chem. Soc.* **2004**, *126*, 12084−12089. (b) Fukuzumi, S.; Kobayashi, T.; Suenobu, T. *Angew. Chem., Int. Ed.* **2011**, *50*, 728−731. (c) Wang, F.; Wang, W. G.; Wang, X. J.; Wang, H. Y.; Tung, C. H.; Wu, L. Z. *Angew. Chem., Int. Ed.* **2011**, *50*, 3193−3197. (d) Probst, B.; Guttentag, M.; Rodenberg, A.; Hamm, P.; Alberto, R. *Inorg. Chem.* **2011**, *50*, 3404−3412. (e) Lakadamyali, F.; Reisner, E. *Chem. Commun.* **2011**, *47*, 1695−1697. (f) Ozawa, H.; Haga, M.; Sakai, K. *J. Am. Chem. Soc.* **2006**, *128*, 4926−4927.

(8) (a) O'Regan, B.; Grätzel, M. *Nature* **1991**, *353*, 737−740. (b) Chen, C. Y.; Chen, J. G.; Wu, S. J.; Li, J. Y.; Wu, C. G.; Ho, K. C. *Angew. Chem., Int. Ed.* **2008**, *47*, 7342−7345. (c) Abbotto, A.; Manfredi, N. *Dalton Trans.* **2011**, *40*, 12421−12438. (d) Kuang, D.; Klein, C.; Ito, S.; Moser, J. E.; Baker, R. H.; Evans, N.; Duriaux, F.; Grätzel, C.; Zakeeruddin, S. M.; Grätzel, M. *Adv. Mater.* **2007**, *19*, 1133−1137.

(9) (a) Bessho, T.; Yoneda, E.; Yum, J.-H.; Guglielmi, M.; Tavernelli, I.; Imai, H.; Rothlisberger, U.; Nazeeruddin, M. K.; Grätzel, M. *J. Am. Chem. Soc.* **2009**, *131*, 5930−5934. (b) Robson, K. C. D.; Koivisto, B. D.; Yella, A.; Sporinova, B.; Nazeeruddin, M. K.; Baumgartner, T.; Grätzel, M.; Berlinguette, C. P. *Inorg. Chem.* **2011**, *50*, 5494−5508. (c) Bomben, P. G.; Gordon, T. J.; Schott, E.; Berlinguette, C. P. *Angew. Chem., Int. Ed.* **2011**, *50*, 10682−10685.

(10) (a) Fernández-Hernández, J. M.; Yang, C. H.; Beltrán, J. I.; Lemaur, V.; Polo, F.; Fröhlich, R.; Cornil, J.; Cola, L. D. *J. Am. Chem. Soc.* **2011**, *133*, 10543−10558. (b) Costa, R. D.; Ortí, E.; Bolink, H. J.; Graber, S.; Housecroft, C. E.; Constable, E. C. *J. Am. Chem. Soc.* **2010**, *132*, 5978−5980. (c) Liu, J.; Liu, Y.; Liu, Q.; Li, C.; Sun, L.; Li, F. *J. Am. Chem. Soc.* **2011**, *133*, 15276−15279. (d) Ladouceur, S.; Fortin, D.; Zysman-Colman, E. *Inorg. Chem.* **2010**, *49*, 5625−5641.

(11) (a) Ulbricht, C.; Beyer, B.; Friebe, C.; Winter, A.; Schubert, U. S. *Adv. Mater.* **2009**, *21*, 4418−4441. (b) Gao, R.; Ho, D. G.; Hernandez, B.; Selke, M.; Murphy, D.; Djurovich, P. I.; Thompson, M. E. *J. Am. Chem. Soc.* **2002**, *124*, 14828−14829.

(12) (a) Goldsmith, J. I.; Hudson, W. R.; Lowry, M. S.; Anderson, T. H.; Bernhard, S. *J. Am. Chem. Soc.* **2005**, *127*, 7502−7510. (b) Lowry, M. S.; Bernhard, S. *Chem.—Eur. J.* **2006**, *12*, 7970−7977. (c) Cline, E. D.; Adamson, S. E.; Bernhard, S. *Inorg. Chem.* **2008**, *47*, 10378−10388. (d) Lowry, M. S.; Goldsmith, J. I.; Slinker, J. D.; Rohl, R.; Pascal, R. A.; Malliaras, G. G.; Bernhard, S. *Chem. Mater.* **2005**, *17*, 5712−5719. (e) DiSalle, B. F.; Bernhard, S. *J. Am. Chem. Soc.* **2011**, *133*, 11819−11821. (f) Chen, T. R.; Lee, H. P.; Chen, J. D. *Inorg. Chem.* **2011**, *50*, 3645−3650.

(13) Wenger, O. S. *Coord. Chem. Rev.* **2009**, *253*, 1439−1457.

(14) Schmid, B.; Garces, F. O.; Watts, R. J. *Inorg. Chem.* **1994**, *33*, 9−14.

(15) (a) Baranoff, E.; Yum, J.-H.; Jung, I.; Vulcano, R.; Grätzel, M.; Nazeeruddin, M. K. *Chem. Asian. J.* **2010**, *5*, 496−499. (b) Baranoff, E.; Yum, J.-H.; Graetzel, M.; Nazeeruddin, M. K. *J. Organomet. Chem.* **2009**, *694*, 2661−2670. (c) Ning, Z.; Zhang, Q.; Wu, W.; Tian, H. *J. Organomet. Chem.* **2009**, *694*, 2705−2711. (d) Mayo, E. I.; Kilså, K.; Tirrell, T.; Djurovich, P. I.; Tamayo, A.; Thompson, M. E.; Lewis, N. S.; Gray, H. B. *Photochem. Photobiol. Sci.* **2006**, *5*, 871−873.

(16) Yuan, Y. J.; Yu, Z. T.; Chen, X. Y.; Zhang, J. Y.; Zou, Z. G. *Chem.—Eur. J.* **2011**, *17*, 12891−12895.

(17) (a) Laskar, I. R.; Chen, T. M. *Chem. Mater.* **2004**, *16*, 111−117. (b) Lo, K. K. W.; Zhang, K. Y.; Chung, C. K.; Kwok, K. Y. *Chem.—Eur. J.* **2007**, *13*, 7110−7120. (c) Chang, W. C.; Hu, A. T.; Duan, J. P.; Rayabarapu, D. K.; Cheng, C. H. *J. Organomet. Chem.* **2004**, *689*, 4882−4888. (d) Djurovich, P. I.; Murphy, D.; Thompson, M. E.; Hernandez, B.; Gao, R.; Hunt, P. L.; Selke, M. *Dalton Trans.* **2007**, *34*, 3763−3770.

(18) Waern, J. B.; Desmarets, C.; Chamoreau, L.-M.; Amouri, H.; Barbieri, A.; Sabatini, C.; Ventura, B.; Barigelletti, F. *Inorg. Chem.* **2008**, *47*, 3340−3348.

(19) (a) Mishra, A.; Fischer, M. K. R.; Bäuerle, P. *Angew. Chem., Int. Ed.* **2009**, *48*, 2474−2499. (b) Ooyama, Y.; Inoue, S.; Nagano, T.;

Kushimoto, K.; Ohshita, J.; Imae, I.; Komaguchi, K.; Harima, Y. *Angew. Chem., Int. Ed.* **2011**, *50*, 7429−7433.
(20) Nelissen, H. F. M.; Feiters, M. C.; Nolte, R. J. M. *J. Org. Chem.* **2002**, *67*, 5901−5906.
(21) Azizi, N.; Amiri, A. K.; Baghi, R.; Bolourtchian, M.; Hashemi, M. M. *Monatsh. Chem.* **2009**, *140*, 1471−1473.
(22) Bae, E. Y.; Choi, W. Y.; Park, J. W.; Kim, H. S.; Lee, J. S. *J. Phys. Chem. B* **2004**, *108*, 14093−14101.
(23) Wang, P.; Zakeeruddin, S. M.; Comte, P.; Charvet, R.; Humphry-Baker, R.; Grätzel, M. *J. Phys. Chem. B* **2003**, *107*, 14336−14341.
(24) (a) Li, X. N.; Wu, Z. J.; Zhang, H. J.; Liu, X. J.; Zhou, L.; Li, Z. F.; Si, Z. J. *Phys. Chem. Chem. Phys.* **2009**, *11*, 6051−6059. (b) Costa, R. D.; Viruela, P. M.; Bolink, H. J.; Ortí, E. *THEOCHEM* **2009**, *912*, 21−26.
(25) Jiang, W.; Gao, Y.; Sue, Y.; Ding, F.; Xu, Y.; Bian, Z.; Li, F.; Bian, J.; Huang, C. *Inorg. Chem.* **2010**, *49*, 3252−3260.
(26) (a) Song, Y. H.; Yeh, S. J.; Chen, C. T.; Chi, Y.; Liu, C. S.; Yu, J. K.; Hu, Y. H.; Chou, P. T.; Peng, S. M.; Lee, G. H. *Adv. Funct. Mater.* **2004**, *14*, 1221−1226. (b) Byun, Y.; Lyu, Y. Y.; Das, R. R.; Kwon, O.; Lee, T. W. *Appl. Phys. Lett.* **2007**, *91*, 211106.
(27) (a) Lo, K. K. W.; Chung, C.-K.; Lee, T. K-M.; Lui, L. H.; Tsang, K. H. K.; Zhu, N. Y. *Inorg. Chem.* **2003**, *42*, 6886−6897. (b) Nasr, G.; Guerlin, A.; Dumur, F.; Baudron, S. A.; Dumas, E.; Miomandre, F.; Clavier, G.; Sliwa, M.; Mayer, C. R. *J. Am. Chem. Soc.* **2011**, *133*, 6501−6504. (c) Yang, C. H.; Cheng, Y. M.; Chi, Y.; Hsu, C. J.; Fang, F. C.; Wong, K. T.; Chou, P. T.; Tsai, M. H.; Wu, C. C. *Angew. Chem., Int. Ed.* **2007**, *46*, 2418−2421.
(28) Xu, M. L.; Zhou, R.; Wang, G. Y.; Xiao, Q.; Du, W. S.; Che, G. B. *Inorg. Chim. Acta* **2008**, *361*, 2407−2412.
(29) (a) Kawamura, Y.; Brooks, J.; Brown, J. J.; Sasabe, H.; Adachi, C. *Phys. Rev. Lett.* **2006**, *96*, 017404. (b) Tsuboyama, A.; Iwawaki, H.; Furugori, M.; Mukaide, T.; Kamatani, J.; Igawa, S.; Moriyama, T.; Miura, S.; Takiguchi, T.; Okada, S.; Hoshino, M.; Ueno, K. *J. Am. Chem. Soc.* **2003**, *125*, 12971−12979.
(30) (a) Sun, J.; Wu, W.; Guo, H.; Zhao, J. *Eur. J. Inorg. Chem.* **2011**, *17*, 3165−3173. (b) Hanson, K.; Tamayo, A.; Diev, V. V.; Whited, M. T.; Djurovich, P. I.; Thompson, M. E. *Inorg. Chem.* **2010**, *49*, 6077−6084. (c) Mak, C. S. K.; Pentlehner, D.; Stich, M.; Wolfbeis, O. S.; Chan, W. K.; Yersin, H. *Chem. Mater.* **2009**, *21*, 2173−2175. (d) Marco, G. D.; Lanza, M.; Pieruccini, M.; Campagna, S. *Adv. Mater.* **1996**, *8*, 576−580.
(31) (a) Thompson, D. W.; Fleming, C. N.; Myron, B. D.; Meyer, T. J. *J. Phys. Chem. B* **2007**, *111*, 6930−6941. (b) Rothe, C.; Chiang, C. J.; Jankus, V.; Abdullah, K.; Zeng, X.; Jitchati, R.; Batsanov, A. S.; Bryce, M. R.; Monkman, A. P. *Adv. Funct. Mater.* **2009**, *19*, 2038−2044.
(32) (a) Neve, F.; Deda, M. L.; Crispini, A.; Bellusci, A.; Puntoriero, F.; Campagna, S. *Organometallics* **2004**, *23*, 5856−5863. (b) Tamayo, A. B.; Garon, S.; Sajoto, T.; Djurovich, P. I.; Tsyba, I. M.; Bau, R.; Thompson, M. E. *Inorg. Chem.* **2005**, *44*, 8723−8732.
(33) Indrakanti, V. P.; Kubicki, J. D.; Schobert, H. H. *Energy Environ. Sci.* **2009**, *2*, 745−758.
(34) (a) Youngblood, W. J.; Lee, S. H. A.; Maeda, K.; Mallouk, T. E. *Acc. Chem. Res.* **2009**, *42*, 1966−1973. (b) Meyer, G. J. *Inorg. Chem.* **2005**, *44*, 6852−6864.
(35) (a) Chou, T. P.; Zhang, Q.; Russo, B.; Fryxell, G. E.; Cao, G. *J. Phys. Chem. C* **2007**, *111*, 6296−6302. (b) Chen, D.; Huang, F.; Cheng, Y. B.; Caruso, R. A. *Adv. Mater.* **2009**, *21*, 2206−2210.